Measuring large-scale structure with the 2dF Galaxy Redshift Survey

J.A. Peacock and the 2dFGRS team*

Institute for Astronomy, University of Edinburgh,
Royal Observatory, Edinburgh EH9 3HJ, UK

Abstract. The 2dF Galaxy Redshift Survey is the first to measure more than 100,000 redshifts. This allows precise measurements of many of the key statistical measures of galaxy clustering, in particular redshift-space distortions and the large-scale power spectrum. This paper presents preliminary 2dFGRS results in these areas.

1 Aims and design of the 2dFGRS

The large-scale structure in the galaxy distribution is widely seen as one of the most important relics from an early stage of evolution of the universe. The 2dF Galaxy Redshift Survey (2dFGRS) was designed to build on previous studies of this structure, with the following main aims:

1. To measure the galaxy power spectrum $P(k)$ on scales up to a few hundred Mpc, bridging the gap between the scales of nonlinear structure and measurements from the the cosmic microwave background (CMB).
2. To measure the redshift-space distortion of the large-scale clustering that results from the peculiar velocity field produced by the mass distribution.
3. To measure higher-order clustering statistics in order to understand biased galaxy formation, and to test whether the galaxy distribution on large scales is a Gaussian random field.

The survey is designed around the 2dF multi-fibre spectrograph on the Anglo-Australian Telescope, which is capable of observing up to 400 objects

* *The 2dF Galaxy Redshift Survey team:* Matthew Colless (ANU), John Peacock (ROE), Carlton M. Baugh (Durham), Joss Bland-Hawthorn (AAO), Terry Bridges (AAO), Russell Cannon (AAO), Shaun Cole (Durham), Chris Collins (LJMU), Warrick Couch (UNSW), Nicholas Cross (St Andrews), Gavin Dalton (Oxford), Kathryn Deeley (UNSW), Roberto De Propris (UNSW), Simon Driver (St Andrews), George Efstathiou (IoA), Richard S. Ellis (Caltech), Carlos S. Frenk (Durham), Karl Glazebrook (JHU), Carole Jackson (ANU), Ofer Lahav (IoA), Ian Lewis (AAO), Stuart Lumsden (Leeds), Steve Maddox (Nottingham), Darren Madgwick (IoA), Peder Norberg (Durham), Will Percival (ROE), Bruce Peterson (ANU), Will Sutherland (ROE), Keith Taylor (Caltech)

simultaneously over a 2 degree diameter field of view. Full details of the instrument and its performance are given in Lewis et al. (2000). See also `http://www.aao.gov.au/2df/`.

The source catalogue for the survey is a revised and extended version of the APM galaxy catalogue (Maddox et al. 1990a,b,c). The extended version of the APM catalogue includes over 5 million galaxies down to $b_{\rm J} = 20.5$ in both north and south Galactic hemispheres over a region of almost $10^4\,{\rm deg}^2$ (bounded approximately by declination $\delta \leq +3$ and Galactic latitude $b \gtrsim 20$). This catalogue is based on Automated Plate Measuring machine (APM) scans of 390 plates from the UK Schmidt Telescope (UKST) Southern Sky Survey. The $b_{\rm J}$ magnitude system for the Southern Sky Survey is defined by the response of Kodak IIIaJ emulsion in combination with a GG395 filter. The photometry of the catalogue is calibrated with numerous CCD sequences and has a precision of approximately 0.2 mag for galaxies with $b_{\rm J} = 17$–19.5. The star-galaxy separation is as described in Maddox et al. (1990b), supplemented by visual validation of each galaxy image.

The survey geometry is shown in Figure 1, and consists of two contiguous declination strips, plus 100 random 2-degree fields. One strip is in the southern Galactic hemisphere and covers approximately $75^\circ \times 15^\circ$ centred close to the SGP at (α, δ)=$(01^h, -30)$; the other strip is in the northern Galactic hemisphere and covers $75^\circ \times 7.5^\circ$ centred at (α, δ)=$(12.5^h, +00)$. The 100 random fields are spread uniformly over the 7000 ${\rm deg}^2$ region of the APM catalogue in the southern Galactic hemisphere. At the median redshift of the survey ($\bar{z} = 0.11$), $100\,h^{-1}\,{\rm Mpc}$ subtends about 20 degrees, so the two strips are $375\,h^{-1}\,{\rm Mpc}$ long and have widths of $75\,h^{-1}\,{\rm Mpc}$ (south) and $37.5\,h^{-1}\,{\rm Mpc}$ (north).

The sample is limited to be brighter than an extinction-corrected magnitude of $b_{\rm J} = 19.45$ (using the extinction maps of Schlegel et al. 1998). This limit gives a good match between the density on the sky of galaxies and 2dF fibres. Due to clustering, however, the number in a given field varies considerably. To make efficient use of 2dF, we employ an adaptive tiling algorithm to cover the survey area with the minimum number of 2dF fields. With this algorithm we are able to achieve a 93% sampling rate with on average fewer than 5% wasted fibres per field. Over the whole area of the survey there are in excess of 250,000 galaxies.

2 Survey Status

By the end of 2000, observations had been made of 161,307 targets in 600 fields, yielding redshifts and identifications for 141,402 galaxies, 7958 stars and 53 QSOs, at an overall completeness of 93%. Repeat observations have been obtained for 10,294 targets. Figure 2 shows the projection of the galaxies in the northern and southern strips onto (α, z) slices. The main points to note

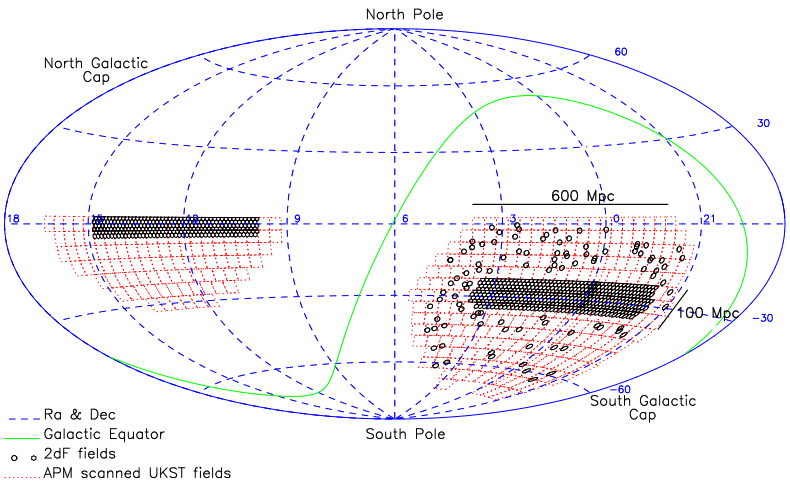

Fig. 1. The 2dFGRS fields (small circles) superimposed on the APM catalogue area (dotted outlines of Sky Survey plates). There are approximately 140,000 galaxies in the $75^\circ \times 15^\circ$ southern strip centred on the SGP, 70,000 galaxies in the $75^\circ \times 7.5^\circ$ equatorial strip, and 40,000 galaxies in the 100 randomly-distributed 2dF fields covering the whole area of the APM catalogue in the south.

are the level of detail apparent in the map and the slight variations in density with R.A. due to the varying field coverage along the strips.

The adaptive tiling algorithm is efficient, and yields uniform sampling in the final survey. However, at this intermediate stage, missing overlaps mean that the sampling fraction has large fluctuations, as illustrated in Figure 3. This variable sampling makes quantification of the large scale structure more difficult, and limits any analysis requiring relatively uniform contiguous areas. However, the effective survey 'mask' can be measured precisely enough that it can be allowed for in low-order analyses of the galaxy distribution.

3 Redshift-space correlations

The simplest statistic for studying clustering in the galaxy distribution is the the two-point correlation function, $\xi(\sigma, \pi)$. This measures the excess probability over random of finding a pair of galaxies with a separation in the plane of the sky σ and a line-of-sight separation π. Because the radial separation in redshift space includes the peculiar velocity as well as the spatial separation, $\xi(\sigma, \pi)$ will be anisotropic. On small scales the correlation function is extended in the radial direction due to the large peculiar velocities in non-linear structures such as groups and clusters – this is the well-known 'Finger-of-God' effect. On large scales it is compressed in the radial direction due to the coherent infall of galaxies onto mass concentrations – the Kaiser effect (Kaiser 1987).

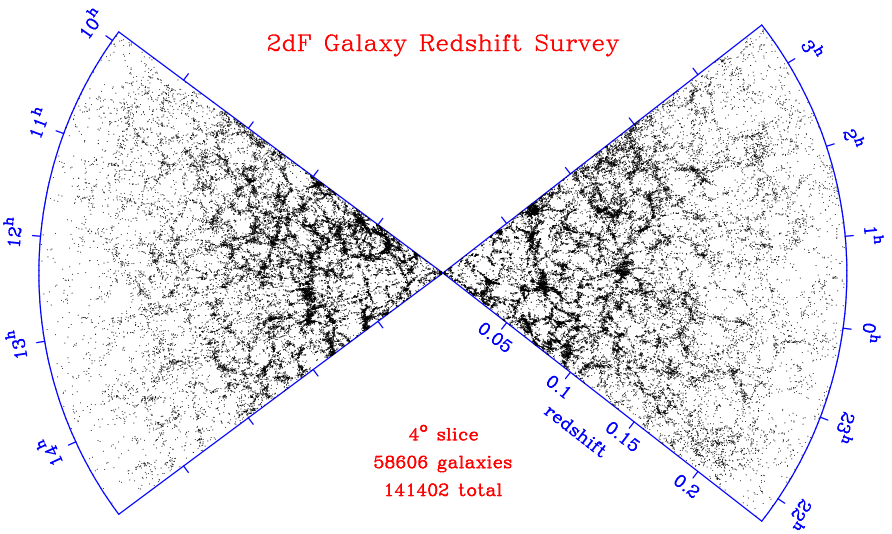

Fig. 2. The distribution of galaxies in part of the 2dFGRS, drawn from a total of 141,402 galaxies: slices 4° thick, centred at declination $-2.5°$ in the NGP and $-27.5°$ in the SGP. Not all 2dF fields within the slice have been observed at this stage, hence there are weak variations of the density of sampling as a function of right ascension. To minimise such features, the slice thickness increases to 7.5° between right ascension 13.1^h and 13.4^h. This image reveals a wealth of detail, including linear supercluster features, often nearly perpendicular to the line of sight. The interesting question to settle statistically is whether such transverse features have been enhanced by infall velocities.

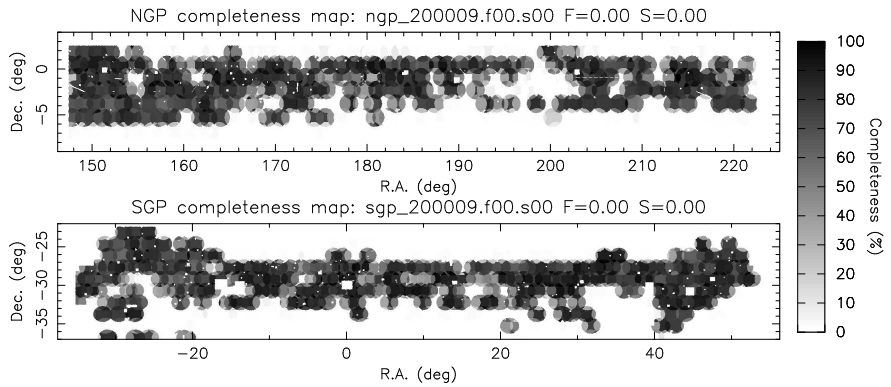

Fig. 3. The completeness as a function of position on the sky. The circles are individual 2dF fields ('tiles'). Unobserved tiles result in low completeness in overlap regions. Rectangular holes are omitted regions around bright stars.

To estimate $\xi(\sigma,\pi)$ we compare the observed count of galaxy pairs with the count estimated from a random distribution following the same selection function both on the sky and in redshift as the observed galaxies. We apply optimal weighting to minimise the uncertainties due to cosmic variance and Poisson noise. This is close to equal-volume weighting out to our adopted redshift limit of $z = 0.25$. We have tested our results and found them to be robust against the uncertainties in both the survey mask and the weighting procedure. The redshift-space correlation function for the 2dFGRS computed in this way is shown in Figure 4. The correlation-function results display very clearly the two signatures of redshift-space distortions discussed above. The 'fingers of God' from small-scale random velocities are very clear, as indeed has been the case from the first redshift surveys (e.g. Davis & Peebles 1983). However, this is the first time that the large-scale flattening from coherent infall has been seen in detail.

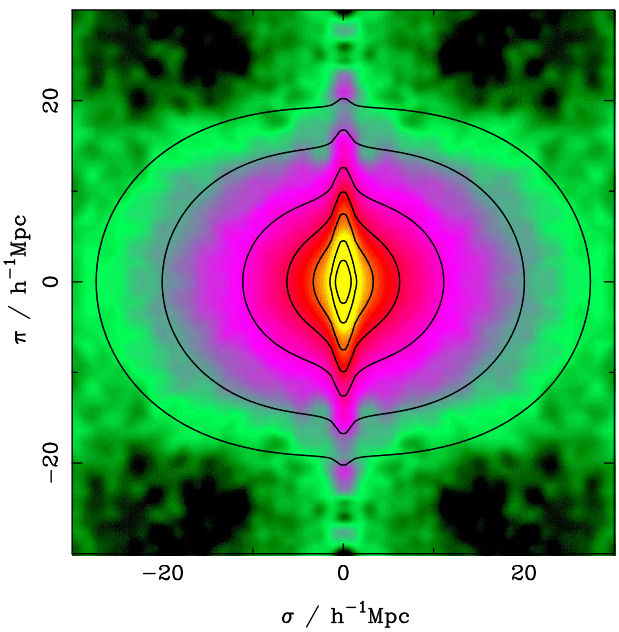

Fig. 4. The galaxy correlation function $\xi(\sigma,\pi)$ as a function of transverse (σ) and radial (π) pair separation is shown as a greyscale image. It was computed in $0.2\,h^{-1}$ Mpc boxes and then smoothed with a Gaussian having an rms of $0.5\,h^{-1}$ Mpc. The contours are for a model with $\beta = 0.4$ and $\sigma_p = 400\,\mathrm{km\,s^{-1}}$, and are plotted at $\xi = 10$, 5, 2, 1, 0.5, 0.2 and 0.1.

The degree of large-scale flattening is determined by the total mass density parameter, Ω, and the biasing of the galaxy distribution. On large scales, it should be correct to assume a linear bias model, so that the redshift-space

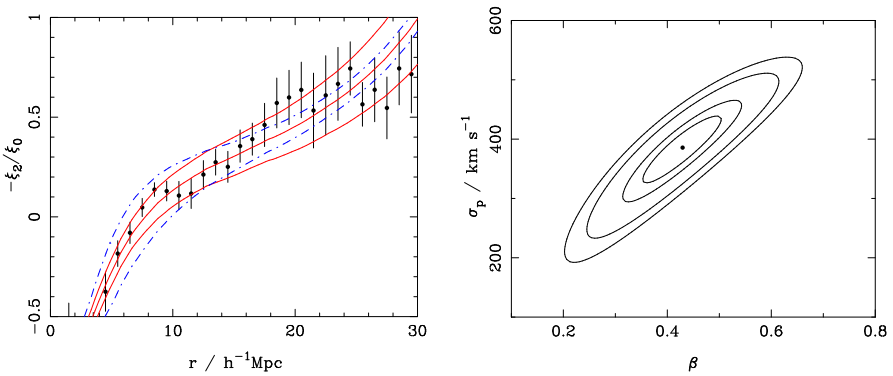

Fig. 5. (a) The compression of $\xi(\sigma,\pi)$ as measured by its quadrupole-to-monopole ratio, plotted as $-\xi_2/\xi_0$. The solid lines correspond to models with $\sigma_p = 400\,\mathrm{km\,s^{-1}}$ and (bottom to top) $\beta = 0.3$,0.4,0.5, while the dot-dash lines correspond to models with $\beta = 0.4$ and (top to bottom) $\sigma_p = 300, 400, 500\,\mathrm{km\,s^{-1}}$. (b) Likelihood contours for β and σ_p from the model fits. The inner contour is the one-parameter 68% confidence ellipse; the outer contours are the two-parameter 68%, 95% and 99% confidence ellipses. The central dot is the maximum likelihood fit, with $\beta = 0.43$ and $\sigma_p = 385\,\mathrm{km\,s^{-1}}$.

distortion on large scales depends on the combination $\beta \equiv \Omega^{0.6}/b$. On these scales, linear distortions should also be applicable, so we expect to see the following quadrupole-to-monopole ratio in the correlation function:

$$\frac{\xi_2}{\xi_0} = \frac{3+n}{n}\,\frac{4\beta/3 + 4\beta^2/7}{1 + 2\beta/3 + \beta^2/5} \qquad (1)$$

where n is the power spectrum index of the fluctuations, $\xi \propto r^{-(3+n)}$. This is modified by the Finger-of-God effect, which is significant even at large scales and dominant at small scales. The effect can be modelled by introducing a parameter σ_p, which represents the rms pairwise velocity dispersion of the galaxies in collapsed structures, σ_p (see e.g. Ballinger et al. 1996). Full details of the fitting procedure are given in Peacock et al. (2000).

Figure 5a shows the variation in ξ_2/ξ_0 as a function of scale. The ratio is positive on small scales where the Finger-of-God effect dominates, and negative on large scales where the Kaiser effect dominates. The best-fitting model (considering only the quasi-linear regime with $8 < r < 25\,h^{-1}\,\mathrm{Mpc}$) has $\beta \simeq 0.4$ and $\sigma_p \simeq 400\,\mathrm{km\,s^{-1}}$; the likelihood contours are shown in Figure 5b. Marginalising over σ_p, the best estimate of β and its 68% confidence interval is

$$\beta = 0.43 \pm 0.07 \qquad (2)$$

This is the first precise measurement of β from redshift-space distortions; previous studies have achieved no more than 3σ detections.

4 Cosmological parameters and the power spectrum

The detailed measurement of the signature of gravitational collapse is the first major achievement of the 2dFGRS; we now consider the quantitative implications of this result. The first point to consider is that there may be significant corrections for luminosity effects. The optimal weighting means that our mean luminosity is high: it is approximately 1.9 times the characteristic luminosity, L^*, of the overall galaxy population (Folkes et al. 1999). Benoist et al. (1996) have suggested that the strength of galaxy clustering increases with luminosity, with an effective bias that can be fitted by $b/b^* = 0.7 + 0.3(L/L^*)$. This effect has been controversial (see Loveday et al. 1995), but the 2dFGRS dataset favours a very similar luminosity dependence. We therefore expect that β for L^* galaxies will exceed our directly measured figure. Applying a correction using the given formula for $b(L)$, we deduce $\beta(L = L^*) = 0.54 \pm 0.09$. Finally, the 2dFGRS has a median redshift of 0.11. With weighting, the mean redshift in the present analysis is $\bar{z} = 0.17$, and our measurement should be interpreted as β at this epoch. The extrapolation to $z = 0$ is model-dependent, but probably does not introduce a significant change (Carlberg et al. 2000).

Our measurement of $\Omega^{0.6}/b$ would thus imply $\Omega = 0.36 \pm 0.10$ if L^* galaxies are unbiased, but it is difficult to justify such an assumption. In principle, the details of the clustering pattern in the nonlinear regime allow the $\Omega - b$ degeneracy to be broken (Verde et al. 1998), but for the present it is interesting to use an independent approach. Observations of CMB anisotropies can in principle measure almost all the cosmological parameters, and Jaffe et al. (2000) obtained the following values for the densities in collisionless matter (c), baryons (b), and vacuum (v): $\Omega_c + \Omega_b + \Omega_v = 1.11 \pm 0.07$, $\Omega_c h^2 = 0.14 \pm 0.06$, $\Omega_b h^2 = 0.032 \pm 0.005$, together with a power-spectrum index $n = 1.01 \pm 0.09$. Our result for β gives an independent test of this picture, as follows.

The only parameter left undetermined by the CMB data is the Hubble constant, h. Recent work (Mould et al. 2000; Freedman et al. 2000) indicates that this is now determined to an rms accuracy of 10%, and we adopt a central value of $h = 0.70$. This completes the cosmological model, requiring a total matter density parameter $\Omega \equiv \Omega_c + \Omega_b = 0.35 \pm 0.14$. It is then possible to use the parameter limits from the CMB to predict a conservative range for the mass power spectrum at $z = 0$, which is shown in Figure 6. A remarkable feature of this plot is that the mass power spectrum appears to be in good agreement with the clustering observed in the APM survey (Baugh & Efstathiou 1994). For each model allowed by the CMB, we can predict both b (from the ratio of galaxy and mass spectra) and also β (since a given CMB model specifies Ω). Considering the allowed range of models, we then obtain the prediction $\beta_{\rm CMB+APM} = 0.57 \pm 0.17$. A flux-limited survey such as the APM will have a mean luminosity close to L^*, so the appropriate comparison is with the 2dFGRS corrected figure of $\beta = 0.54 \pm 0.09$ for L^* galaxies. These numbers are in very close agreement. In the future, the value of β will become

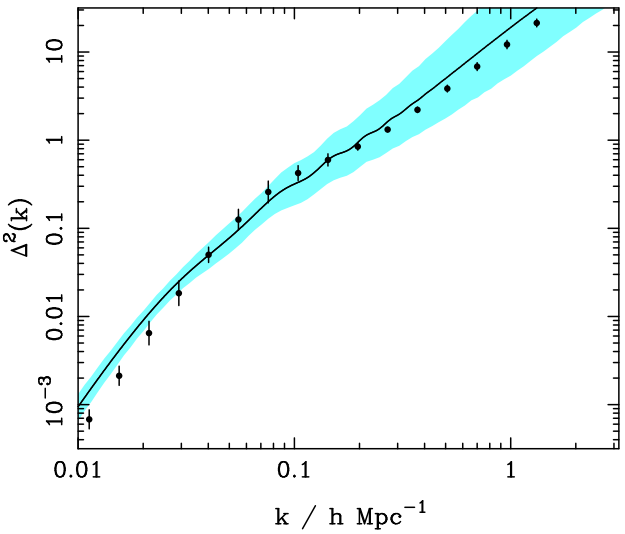

Fig. 6. The dimensionless matter power spectrum at zero redshift, $\Delta^2(k)$, as predicted from the allowed range of models that fit the microwave-background anisotropy data, plus the assumption that $H_0 = 70\,\mathrm{km\,s^{-1}Mpc^{-1}} \pm 10\%$. The solid line shows the best-fit model from Jaffe et al. (2000) [power-spectrum index $n = 1.01$, and density parameters in baryons, CDM, and vacuum of respectively 0.065, 0.285, 0.760]. The effects of nonlinear evolution have been included, according to a revised version of the procedure of Peacock & Dodds (1996). The shaded band shows the 1σ variation around this model allowed by the CMB data. The solid points are the real-space power spectrum measured for APM galaxies. The clear conclusion is that APM galaxies are consistent with being essentially unbiased tracers of the mass on large scales.

one of the most direct ways of confronting large-scale structure with CMB studies.

5 The 2dFGRS power spectrum

Of course, one may question the adoption of the APM power spectrum, which was deduced by deprojection of angular clustering. The 3D data of the 2dFGRS should be capable of improving on this determination, and we have made a first attempt at doing this, shown in Figure 7.

This power-spectrum estimate uses the FFT-based approach of Feldman, Kaiser & Peacock (1994), and needs to be interpreted with care. Firstly, it is a raw redshift-space estimate, so that the power beyond $k \simeq 0.2\,h\,\mathrm{Mpc}^{-1}$ is severely damped by fingers of God. On large scales, the power is enhanced, both by the Kaiser effect and by the luminosity-dependent clustering discussed above. Finally, the FKP estimator yields the true power convolved with the window function. This modifies the power significantly on large

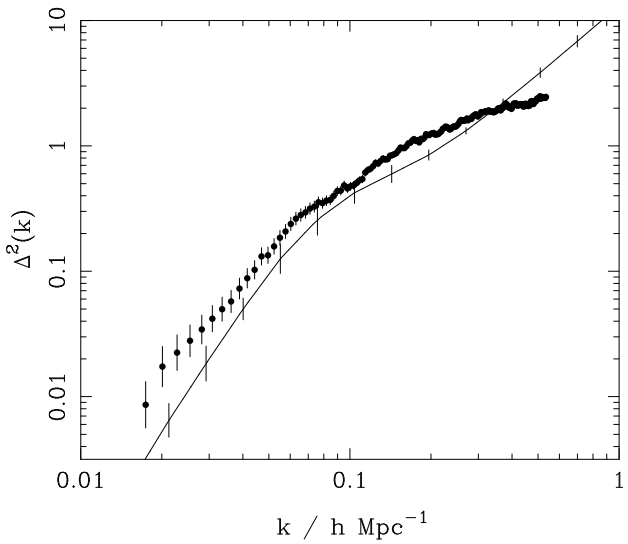

Fig. 7. The 2dFGRS redshift-space power spectrum, estimated according to the FKP procedure. The solid points with error bars show the power estimate. The window function correlates the results at different k values, and also distorts the large-scale shape of the power spectrum An approximate correction for the latter effect has been applied. The line shows the real-space power spectrum estimated by deprojection from the APM survey.

scales (roughly a 20% correction). We have made an approximate correction for this by multiplying by the correction factor appropriate for a $\Gamma = 0.25$ CDM spectrum. The precision of the power measurement appears to be encouragingly high, and the systematic corrections from the window are well specified. the next task will be to perform a detailed fit of physical power spectra, taking full account of the window effects. The hope is that we will obtain not only a more precise measurement of the overall spectral shape, as parameterized by Γ, but will be able to move towards more detailed questions such as the existence of baryonic features in the matter spectrum (Meiksin, White & Peacock 1999).

6 Conclusions

The 2dFGRS is now the largest 3D survey of the local universe, by a factor of over 5. When it is complete, we expect to have obtained definitive results on a number of key issues relating to galaxy clustering. For details of the current status of the 2dFGRS, see `http://www.mso.anu.edu.au/2dFGRS`. In particular, this site gives details of the 2dFGRS public release policy, in which we intend to release approximately the first half of the survey data by mid-2001, with the complete survey database to be made public by mid-2003.

References

Ballinger W.E., Peacock J.A., Heavens A.F., 1996, MNRAS, 282, 877
Baugh C.M., Efstathiou G., 1994, MNRAS, 267, 323
Benoist C., Maurogordato S., da Costa L.N., Cappi A., Schaeffer R., 1996, ApJ, 472, 452
Carlberg R.G., Yee H.K.C., Morris S.L., Lin H., Hall P.B., Patton D., Sawicki M., Shepherd C.W., 2000, ApJ, 542, 57
Davis M., Peebles, P.J.E., 1983, ApJ, 267, 465
Folkes S.J. et al., 1999, MNRAS, 308, 459
Feldman H.A., Kaiser N., Peacock J.A., 1994, ApJ, 426, 23
Freedman W.L. et al., 2000, astro-ph/0012376
Jaffe A. et al., 2000, astro-ph/0007333
Kaiser N., 1987, MNRAS, 227, 1
Lewis I., Taylor K., Cannon R.D., Glazebrook K., Bailey J.A., Farrell T.J., Lankshear A., Shortridge K., Smith G.A., Gray P.M., Barton J.R., McCowage C., Parry I.R., Stevenson J., Waller L.G., Whittard J.D., Wilcox J.K., Willis K.C., 2000, MNRAS, submitted
Loveday J., Maddox S.J., Efstathiou G., Peterson B.A., 1995, ApJ, 442, 457
Maddox S.J., Efstathiou G., Sutherland W.J., Loveday J., 1990a, MNRAS, 242, 43P
Maddox S.J., Sutherland W.J., Efstathiou G., Loveday J., 1990b, MNRAS, 243, 692
Maddox S.J., Efstathiou G., Sutherland W.J., 1990c, MNRAS, 246, 433
Meiksin A.A., White M., Peacock J.A., 1999, MNRAS, 304, 851
Mould J.R. et al., 2000, ApJ, 529, 786
Peacock J.A., Dodds S.J., 1996, MNRAS, 280, L19
Peacock J.A. et al., 2000, Nature, submitted
Schlegel D.J., Finkbeiner D.P., Davis M., 1998, ApJ, 500, 525
Verde L., Heavens A.F., Matarrese S., Moscardini L., 1998, MNRAS, 300 747